Conference Proceedings

EuroSun 2016
Palma de Mallorca (Spain), 11 - 14 October 2016

Erosion experimental system design and experimental research of high temperature molten salt

Yao Fan[1], Bi Qincheng[1]

[1] The State Key Laboratory of Multiphase Flow in Power Engineering, Xi'an Jiaotong University, Xi'an 710049, China

Abstract

The erosion behavior of two types of stainless steel in mixtures of sodium nitrate ($NaNO_3$) and potassium nitrate (KNO_3) is presented. The erosion resistance can be used to evaluate the lifetime of heat exchange tubes for solar thermal applications. A molten salt erosion experimental system was established for this purpose. Erosion tests were conducted for approximately 750 hours with type 304 and 321 stainless steel at 500 ºC and 400 ºC with different molten salt wash velocities, ranging from 1.09 m/s to 2.98 m/s. Erosion rates were determined by mass losses, and the results indicate that short-term erosion rates of the two types of stainless steel can be described in term of parabolic kinetics. The annual rates of metal loss were measured to be 10.8 to 18 μm/year for 304 stainless steel at 500 ºC depending on the wash velocities. Metal loss for 321 stainless steel at 500 ºC is about 7.68 to 10.92 μm/year. Based on these results, we confirm that the erosion resistance performance of 321 stainless steel is better than that of 304, which may be related to the titanium in 321 stainless steel.

Keywords: *Erosion behavior, molten salt, 321stainless steel, 304stainless steel*

1. Introduction

The two primary components of Concentrated Solar Power (CSP) are the receiver and heat exchanger. In a CSP system, the receiver structure consists of tubing panels through which heat transfer fluid circulates as it is heated by sunlight focused by an array of computer-controlled mirrors. The heat exchanger constitutes of a number of tubes transferring heat in fluid cross-flow tube banks that is steam cooled on the tube side. It has been suggested that a higher performance material should be used to construct these devices, such as stainless steel. We chose to study 300 series stainless steels; previous work has demonstrated that they exhibit good corrosion resistance and no degradation in mechanical properties after relatively long-term exposure to molten nitrates at the temperatures of interest.

The chosen heat transfer fluid is one of the most important aspects of a successfully operating power plant. Solar Two utilizes a molten salt consisting of 60 wt.% $NaNO_3$ and 40 wt.% KNO_3 as the heat transfer fluid, which has a melting point of 238 ºC and an intended working range of 290 ºC to 560 ºC. This mixture optimizes a number of important properties, including heat capacity, thermal conductivity, corrosivity, ease of handling and storage, and cost.

While the previous studies mentioned above have established the static corrosion behavior of stainless steel immersed in molten salt, there is little information regarding the dynamic erosion behavior at different flow rates of molten salt. Recent papers concerning stainless steel immersed in different mixtures of molten salt reported that pitting type corrosion occurs on the material's surface. Pitting corrosion of stainless steel is a critical form of corrosion in engineering structures and most equipment fabricated from stainless steel fail due to pitting. Moreover, the flow rates of molten salt could aggravate pitting corrosion. Therefore, the dynamic erosion behavior may be worse than static corrosion behavior. One specific goal of the current work is to address the question of molten salt velocity on corrosivity.

doi:10.18086/eurosun.2016.06.05 Available at http://proceedings.ises.org

2. System description

In order to research the dynamic erosion behavior of heat exchanger tubes at high temperature due to molten salt, the author independently designed and established a high temperature molten salt erosion experimental system, as shown in Fig. 1 and Fig. 2.

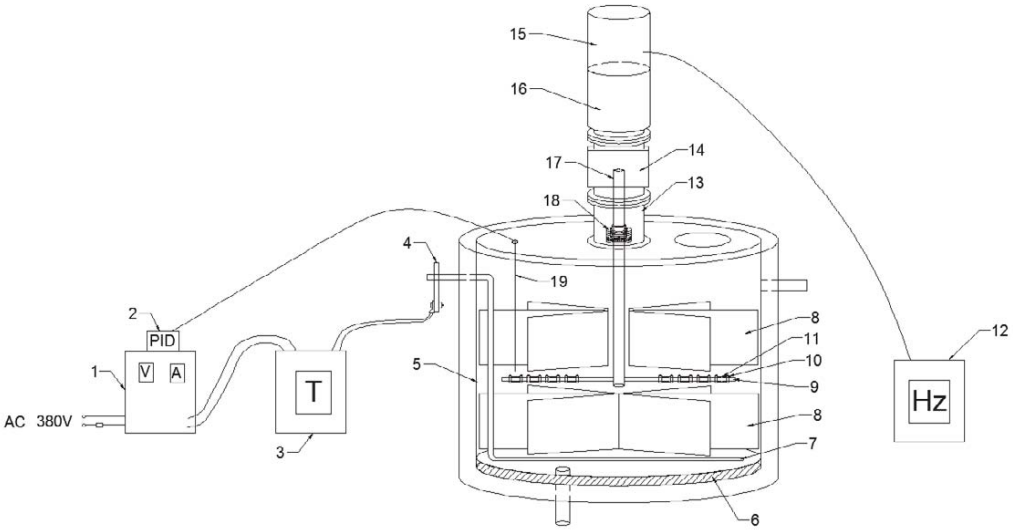

Fig. 1: Experimental system diagram 1：SCR voltage regulator；2：PID regulator；3：transformer；4：electrode plate；5：molten salt storage can；6：fire brick；7：heating element； 8：baffle；9：agitating shaft；10：ferrule ；11：experimental test；12：inverter；13：metal stent；14：reducer；15：encoder；16：motor；17：motor shaft；18：coupling；19：thermocouple

Fig. 2: Experimental system picture

The high temperature molten salt erosion experimental system consisted of an electrical heating system and erosion system. The electrical heating box was made of thick stainless steel for the internal surface, a middle layer filled with insulating cotton and an external surface containing an iron sheet. A layer of firebricks was spread on the bottom of electrical heating box. Two terminals of heating tubes were placed on the firebrick directly by welding with electrical heating plates. Ceramic tubes acted as insulators between the extension of the heating tube and electrical heating box. The transformer was connected with a silicon controlled voltage regulator by cable. One side of the cable was connected with electrical heating plates by four screws; the other side was link with a transformer. The silicon controlled voltage regulator includes a voltmeter,

amperage meter and PID controller. PID controller adjusted the output current from the silicon controlled voltage regulator in real time and controlled the heating power of the entire system by receiving a temperature signal from the sensors. The other side of the silicon controlled voltage regulator was linked to a 380 V alternating current by cable connections, which were installed with an electrical leakage protector to prevent short-circuiting. The erosion system was comprised of a motor shaft with accessory components. One side of the motor shaft was immersed in molten salt and installed as an agitating shaft. Coupons were installed on the agitating shaft according to the expected design distance are shown in Fig. 3. Both sides of the coupons were locked by card sleeves to prevent rolling while the agitating shaft was moving.

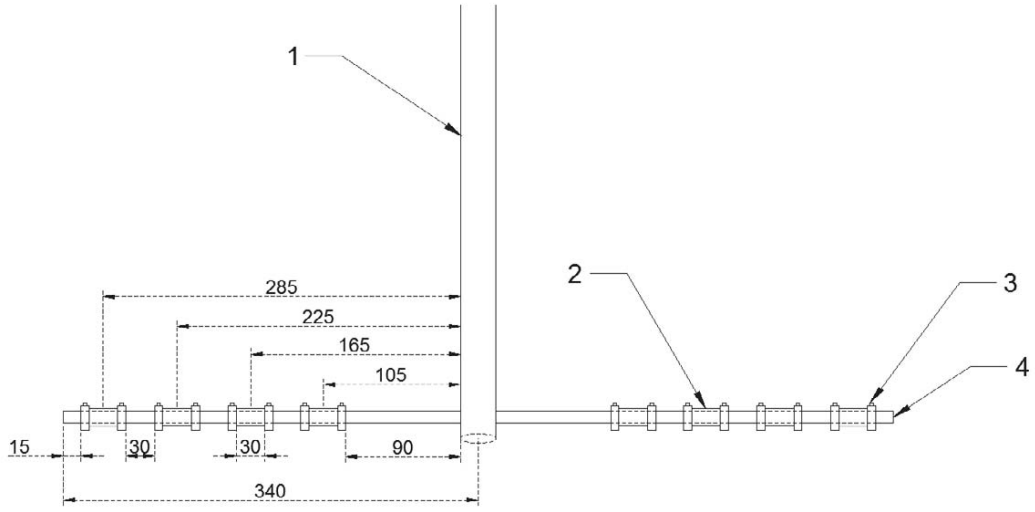

Fig. 3: Testing section distributions

1：motor shaft；2：experiment test；3：ferrule；4：agitating shaft

A coupling was installed on an extension from the motor shaft's electrical heating box. The upper side of the coupling was connected with the motor shaft using a keyway structure and a thrust bearing supported the bottom side. The motor shaft was connected with a reducer. The other side of the reducer was connected to a motor. The top of the motor was set up with an encoder, which was linked to a frequency converter, by signal wires. Baffles were installed on both sides of the agitating shaft in the electrical heating box in order to decrease the effect of turbulent flow in the vertical direction. The rotation speed of the motor was controlled by adjusting the operation panel of the frequency converter. This control allowed us to simulate the erosion behavior of stainless steels at different velocities of molten salt. In this experiment, the rotated speed of motor was set to 100 $r \cdot min^{-1}$, moreover the calculated velocities of each coupon are reported in Table 1. For maintaining precise experimental temperature, the thermocouple was installed on the same flat surface with the coupons.

Tab. 1: Locations and velocities of coupons

Number	Radius(m)	Velocity($m \cdot s^{-1}$)
1	0.105	1.099
2	0.165	1.727
3	0.225	2.355
4	0.285	2.983

Based on the commercial applications of the heat exchanger, we chose two types of stainless steel (SS) as coupons: 304SS and 321SS. The coupons, measuring approximately 30 mm × 25 mm× 3 mm in thickness, were cut from stainless steel tubes, polished, cleaned, alcohol rinsed, and weighed prior to immersion in salt. Two specimens of each alloy were immersed at 500 ºC and removed from nitrate mixtures at intervals of 168, 336, 504, and 720 hours for examination and analysis. Before starting the analysis the samples were washed

in distilled water, and cleaned ultrasonically in alcohol. The coupons were weighed after immersion to measure loss due to erosion process.

3. Data collection and discussion

Corrosion kinetics refers to the variable quantity of coupons per unit area in the experimental process. This study provides descaled mass loss measurements per unit area after conducting analysis and calculations. Mass loss measurements are an easy and direct way to represent the erosion behavior. Dissolvability of corrosion products and corrosion product adsorption onto coupons were not considered. Next, values of M are established using the descaled mass loss of metal alloys according to Equation. 1.

$$M = \frac{W_0 - W_1}{S} \qquad \text{(eq. 1)}$$

In Equation 1, M is the descaled mass loss of coupons per unit area. W_0 and W_1 represent the original mass and the post-experiment mass of coupons, respectively, and S is the surface-area of coupons. In this case, the value of S is 23.55 cm^2.

Adding the time factor to the Equation 1, the descaled mass loss of coupons per unit interval (erosion rate) is calculated according to Equation. 2.

$$V = \frac{W_0 - W_1}{S * t} \qquad \text{(eq. 2)}$$

In Equation 2, V is the erosion rates of coupons and t is the erosion time.

Fig. 4 is a plot of the average mass loss data versus time for 304SS based on different molten salt velocities. The mass losses were between 1.08 and 1.76 mg/cm^2 after 720 hours of erosion. The kinetics appear closely to follow parabolic rate laws initially and later become linear after prolonged exposures. In the absence of uniform erosion kinetics for the entire duration of coupon immersion, a conservative approach based on a linear extrapolation of the data seems warranted for estimating erosion-induced metal loss over longer timescales. For 500 ºC isothermal exposures, such linear extrapolations yield annualized mass losses of 12.96-21.12 mg/cm^2. We emphasize that these estimates are based on the flow velocity of molten salt used in this experiment.

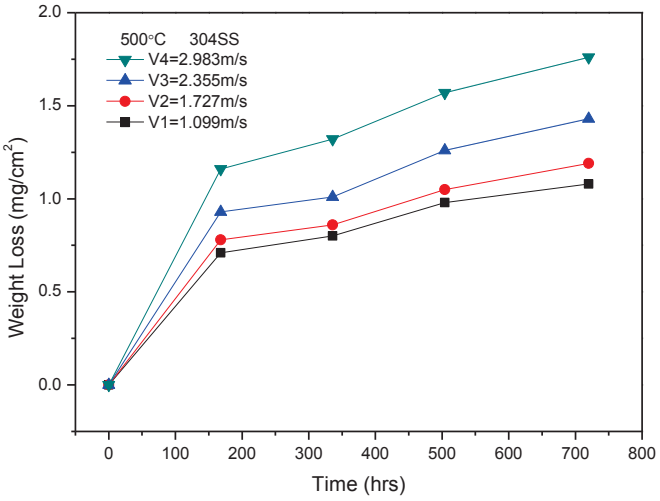

Fig. 4: Descaled weight loss measurements for 304 stainless steel specimens exposed to nitrate salt mixtures at 500 ºC

Based on Fig. 5, mass loss rate curve can be clearly observed. Mass loss velocities were $6.9 \cdot 10^{-3}$ mg·cm^2·h^{-1} after 168 hours and $2.4 \cdot 10^{-3}$ mg·cm^2·h^{-1} after 720 hours with a molten salt flow velocity of 2.983 m/s. Therefore, we hypothesize that steel erosion is based on a high corrosion rate at the beginning of the experiment and decreases slightly as time elapses. The erosion rate then became constant and dropped to a minimum erosion rate. The corrosion is possibly due to chemical or electrochemical processes that take place on the surface of the material. The electrochemical reaction is reduction and oxidation or can be simplified as a redox coupled reaction. Metal and alloy were used to form an oxide layer on the metal surface in air. The oxide layer is responsible for protecting the surface and retarding diffusion of oxidants to the reaction interface of the metal or alloy. The 304 stainless steel, with chromium and iron ions, tends to form Cr_2O_3 and Fe_2O_3 as its protective oxide layer. After a period of time, the coupons are immersed in molten salt, and anions will gather at points on the surface of coupons; moreover, certain points have negative potential. Electrons will move between certain anions points and their surroundings due to the potential difference, as if forming primary cells. The Cr_2O_3 and Fe_2O_3 of the protective oxide layer and iron atoms will exchange in an ionic state dissolved in molten salt. This reaction can induce pitting type erosion and cause an interruption or breakdown of the protective oxide film on the surface of the metal. The high corrosion rate at the beginning is likely due to impurities on the surface of coupons, such as carbon, which are prone to induce the redox reaction. After the conclusion of impurity reactions, the erosion rate is reduced with time. We hypothesize that the minimum erosion rate is achieved once the erosion rate is equal to the protective oxide layer self-regeneration.

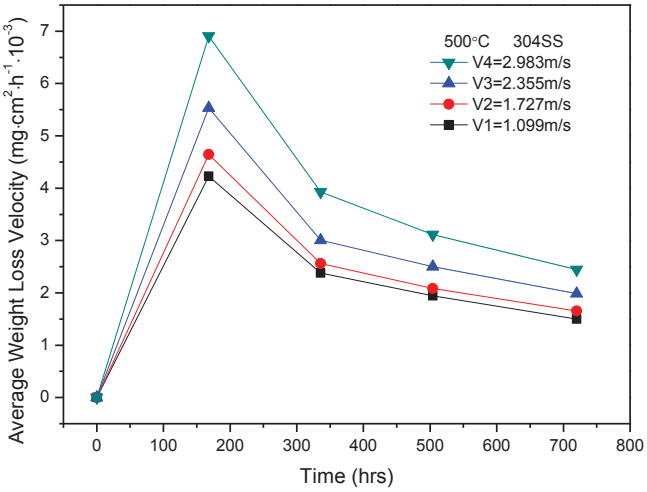

Fig. 5: Descaled weight loss velocity measurements for 304 stainless steel specimens exposed to nitrate salt mixtures at 500 ºC

Descaled mass loss measurements for 321SS coupons removed from nitrate salt mixtures at different flow velocities and 500 ºC are presented in Fig. 6. The mass losses range from 0.78 to 1.29 mg/cm^2 after 720 hours of immersion. Overall, 321SS exhibited more effective erosion resistance compared to 304SS. The mass loss data for 321SS reveal differences due to titanium. The 321 stainless steel has chromium, titanium and iron ions, which form Cr_2O_3, Ti_2O_3 and Fe_2O_3 as its protective oxide layer. According to standard electrode potentials shown in Table 2, the standard electrode potential of chromium is higher than that of titanium and the standard electrode potential of iron is highest of the three elements.

Tab. 2: Standard electrode potentials (25 ºC, 101.325kPa)

Number	Electrode process	Standard electrode potential(V)
1	Fe^{3+}+3e═Fe	-0.037
2	Cr^{3+}+3e═Cr	-0.744
3	Ti^{3+}+3e═Ti	-1.37

The higher the standard electrode potential element, the stronger its ability to capture electrons in the element's oxidation state. The Cr_2O_3 and Fe_2O_3 conduct electrochemical reaction captures electrons when the accumulation of ionic potential on the surface of coupons is higher than the equilibrium potential of chromium. This reaction deteriorates the protective oxide layer. However, this potential is too low for Ti_2O_3 to respond. The Ti_2O_3 electrochemical reaction proceeds when the accumulation of ionic potential on the surface of coupons is higher than the equilibrium potential of titanium. Therefore, the protective oxide layer of titanium has a more effective erosion resistance performance.

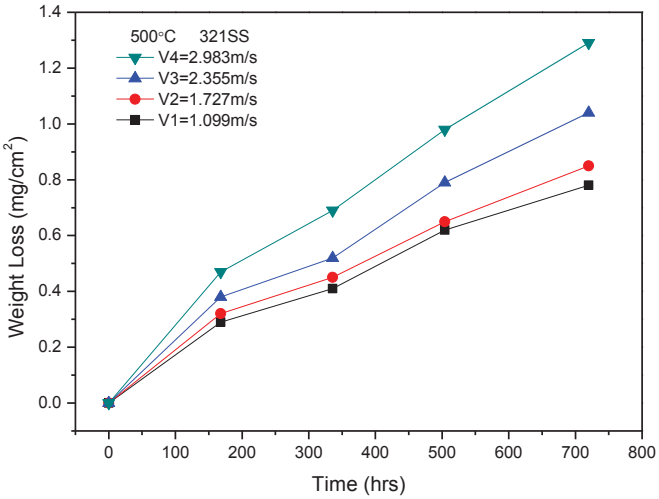

Fig. 6: Descaled weight loss measurements for 321 stainless steel specimens exposed to nitrate salt mixtures at 500 ºC

The descaled mass loss rate data for 321SS due to molten salt at different flow velocities and 500 ºC are shown in Fig. 7. Mass loss rates were $2.8 \cdot 10^{-3}$ mg·cm^2·h^{-1} after 168 hours and $1.8 \cdot 10^{-3}$ mg·cm^2·h^{-1} after 720 hours at 2.983 m/s molten salt flow velocity. The erosion rates curve for 321SS also generally shows slower rates after the initial high erosion rate. On the whole, the lower erosion rates for 321SS coupons than that of 304SS coupons potentially demonstrates that 321SS erosion resistance is stronger than 304SS erosion resistance.

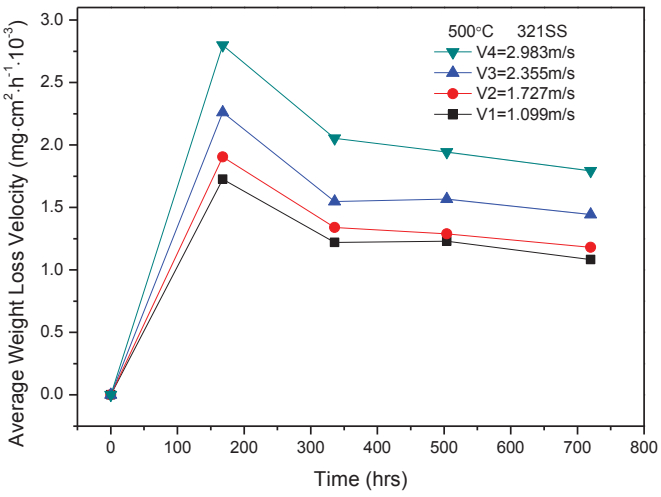

Fig. 7: Descaled weight loss velocity measurements for 321 stainless steel specimens exposed to nitrate salt mixtures at 500 ºC

4. Conclusions

The 300 series stainless steels are the most important materials to be used in solar thermal applications. The experimental data presented in this study indicate that flow velocities and temperature of molten salt play important roles in the erosion process of stainless steel. For the two sets of coupons made from different types of stainless steel, both rate of mass losses increased as flow velocities increased. However, erosion rates for SS321 were less sensitive to molten salt flow velocities than that of 304SS, due to the presence of titanium, which provides a protective oxide layer on the surface. The erosion kinetics of SS304 present a parabolic tendency, while that of SS321 exhibit approximately a linear one. Future work on the influence of different molten salt compositions on erosion behavior is warranted, in order to further develop an understanding of erosion behavior of 304SS and 321SS.

5. References

R. W. Bradshaw and R. W. Carling., 1987. A Review of the Chemical and Physical Properties of Molten Alkali Nitrate Salts and Their Effect on Materials Used for Solar Central Receivers, Sandia National Laboratories.

Cristina Prieto, Laia Miró, Gerard Peiró, Eduard Oró, Antoni Gil, & Luisa F. Cabeza, 2016, Temperature Distribution and Heat Losses in Molten Salts Tanks for CSP Plants, Solar Energy, Vol. 135, 518–526

Cabeza, L. F., & Mehling, H., 2003. Review On Thermal Energy Storage With Phase Change: Materials, Heat Transfer Analysis And Applications., Vol. 23, pp. 251-283

I.B. Singh, 1995, The Influence of Moisture on the Oxidation Rate of Iron in NaNO3 and KNO3 Melts, Corrosion Science, pp. 1981–1989

Brashaw, R. W., & Siegel, N. P., 2008. Molten Nitrate Salt Development for Thermal Energy Storage in Parabolic Trough Solar Power System, 1-7.

Ebner, M. A., Sharpe, P., & Sharpe, P. 2010. Engineering Database of Liquid Salt Thermophysical and Thermochemcal Properties Engineering Database of Liquid Salt Thermophysical.

Raade, J. W., Padowitz, D., & Vaughn, J., 2011. Low Melting Point Molten Salt Heat Transfer Fluid With Reduced Cost. I.

S. Guillot, A. Faik, A. Rakhmatullin, J. Lambert, E. Veron, P. Echegut, C. Bessada, N. Calvet, X. Py, 2012, Corrosion Effects Between Molten Salts and Thermal Storage Material for Concentrated Solar Power Plants, Applied Energy, pp. 174–181

F. Javier Ruiz-Cabañas, Cristina Prieto, Rafael Osuna, Virginia Madina, 2016, Corrosion Testing Device for In-situ Corrosion Characterization in Operational Molten Salts Storage Tanks: A516 Gr70 Carbon Steel Performance under Molten Salts Exposure, Solar Energy Materials and Solar Cells, Vol 157, 383-392

Fontana, M. G. and Green, N. D, 1967. Corrsion Engineering. New York, McGraw-Hill. 51.

Jongnotte, B. J., 2007. Stainless steel in architectural construction, beautiful but delicate.

Ma, F., 2012. Corrosive Effects of Chlorides on Metals, 178.

Wei-Jen Cheng, Ding-Jhih Chen, Chaur-Jeng Wang, 2015, High-temperature Corrosion of Cr-Mo Steel in Molten LiNO3-NaNO3-KNO3 Eutectic Salt for Thermal Energy Storage, Solar Energy Materials and Solar Cells, Vol 132, 563-569

I.B. Singh, 1992, Influence of Temperature and Sulphate Ion on Corrosion of Mild Steel in Molten NaNO3, British Corrosion Journal, pp. 299–304

I.B. Singh, 1993, The Effect of NaCI Addition on the Corrosion of Mild Steel in NaNO3 Melt, Corrosion Science, pp. 1733–1742

Taltavull, C., Shi, Z., Torres, B., Rams, J., & Atrens, A. 2014. Influence of the chloride ion concentration on the corrosion of high-purity Mg, ZE41 and ZA91 in buffered Hank's solution. Journal of materials science. Materials in medicine, 329-45.

A.G. Fernández, H. Galleguillos, & F.J. Pérez, 2014, Thermal Influence in Corrosion Properties of Chilean Solar Nitrates, Solar Energy, Vol 109, 125–134

Geoff McConohy, Alan Kruizenga, 2014,Molten Nitrate Salts at 600 and 680 °C: Thermophysical Property Changes and Corrosion of High-temperature Nickel Alloys, Solar Energy, Vol 103, 242–252

R.W. Bradshaw, S.H. Goods, Corrosion Resistance of Stainless Steels During Thermal Cycling in Alkali

Nitrate Molten Salts, SAND2001-8518
R.W. Bradshaw, S.H. Goods, Corrosion Resistance of Nickel-Base Alloys in Molten Alkali Nitrates, SAND2000-8240.
S.H. Goods, R.W. Bradshaw, M.R. Prairie, J.M. Chavez, Corrosion of Stainless and Carbon Steels in Molten Mixtures of Industrial Nitrates, SAND94-8211.